nature genetics

ANKS6 is a central component of a nephronophthisis module linking NEK8 to INVS and NPHP3

Sylvia Hoff[1–3,28], Jan Halbritter[4,28], Daniel Epting[1], Valeska Frank[5], Thanh-Minh T Nguyen[6], Jeroen van Reeuwijk[6], Christopher Boehlke[1], Christoph Schell[1–3], Takayuki Yasunaga[1], Martin Helmstädter[1,3], Miriam Mergen[1], Emilie Filhol[7,8], Karsten Boldt[9], Nicola Horn[9], Marius Ueffing[9,10], Edgar A Otto[11], Tobias Eisenberger[5], Mariet W Elting[12], Joanna A E van Wijk[13], Detlef Bockenhauer[14], Neil J Sebire[15], Søren Rittig[16], Mogens Vyberg[17], Troels Ring[18], Martin Pohl[19], Lars Pape[20], Thomas J Neuhaus[21], Neveen A Soliman Elshakhs[22], Sarah J Koon[23], Peter C Harris[23], Florian Grahammer[1], Tobias B Huber[1,24], E Wolfgang Kuehn[1,24], Albrecht Kramer-Zucker[1], Hanno J Bolz[5,25], Ronald Roepman[6], Sophie Saunier[7,8], Gerd Walz[1,24], Friedhelm Hildebrandt[4,26], Carsten Bergmann[1,5,27] & Soeren S Lienkamp[1]

Nephronophthisis is an autosomal recessive cystic kidney disease that leads to renal failure in childhood or adolescence. Most NPHP gene products form molecular networks. Here we identify ANKS6 as a new NPHP family member that connects NEK8 (NPHP9) to INVS (NPHP2) and NPHP3. We show that ANKS6 localizes to the proximal cilium and confirm its role in renal development through knockdown experiments in zebrafish and *Xenopus laevis*. We also identify six families with *ANKS6* mutations affected by nephronophthisis, including severe cardiovascular abnormalities, liver fibrosis and *situs inversus*. The oxygen sensor HIF1AN hydroxylates ANKS6 and INVS and alters the composition of the ANKS6-INVS-NPHP3 module. Knockdown of *Hif1an* in *Xenopus* results in a phenotype that resembles loss of other NPHP proteins. Network analyses uncovered additional putative NPHP proteins and placed ANKS6 at the center of this NPHP module, explaining the overlapping disease manifestation caused by mutation in *ANKS6*, *NEK8*, *INVS* or *NPHP3*.

Nephronophthisis is the most frequent genetic cause of renal failure in children, presenting with cystic kidney disease combined with extrarenal manifestations, such as retinitis pigmentosa (Senior-Løken syndrome), liver fibrosis, cerebellar vermis hypoplasia (Joubert syndrome), *situs inversus* or cardiac malformations[1,2]. Because most NPHP gene products localize to the cilium or its associated structures, nephronophthisis and related syndromes, such as Joubert syndrome and Meckel-Gruber syndrome (MKS), have been termed ciliopathies[3]. Although more than a dozen causative genes have been identified, an unexpectedly large proportion of individuals with nephronophthisis (approximately 60%) do not have a mutation in any of the known genes[4]. Most NPHP proteins have domain architectures typical of adaptor molecules involved in protein-protein interactions and form large protein networks[5,6]. Hence, a remaining challenge is to identify the missing components in order to understand how these protein complexes exert their developmental and tissue-specific functions. Although NPHP members engage in multiple protein-protein interactions, four distinct subnetworks have been identified: the NPHP1-NPHP4-NPHP8 module, the NPHP5-NPHP6 module,

[1]Department of Medicine, Renal Division, University of Freiburg Medical Center, Freiburg, Germany. [2]Spemann Graduate School of Biology and Medicine (SGBM), Albert-Ludwigs-University Freiburg, Freiburg, Germany. [3]Faculty of Biology, Albert-Ludwigs-University Freiburg, Freiburg, Germany. [4]Department of Medicine, Boston Children's Hospital, Harvard Medical School, Boston, Massachusetts, USA. [5]Center for Human Genetics, Bioscientia, Ingelheim, Germany. [6]Department of Human Genetics, Nijmegen Centre for Molecular Life Sciences and Institute for Genetic and Metabolic Disease, Radboud University Medical Centre, Nijmegen, The Netherlands. [7]Institute National de la Santé et de la Recherche Médicale (INSERM) U983, Hôpital Necker–Enfants Malades, Paris, France. [8]Paris Descartes–Sorbonne Paris Cité University, Imagine Institute, Paris, France. [9]Institute for Ophthalmic Research, Division of Experimental Ophthalmology and Medical Proteome Center, University of Tuebingen, Tuebingen, Germany. [10]Research Unit Protein Science, Helmholtz Zentrum München–German Research Center for Environmental Health, Munich and Neuherberg, Germany. [11]Department of Pediatrics, University of Michigan, Ann Arbor, Michigan, USA. [12]Department of Clinical Genetics, VU University Medical Center, Amsterdam, The Netherlands. [13]Department of Pediatric Nephrology, VU University Medical Center, Amsterdam, The Netherlands. [14]University College London (UCL) Institute of Child Health and Pediatric Nephrology, Great Ormond Street Hospital, London, UK. [15]Department of Histopathology, Great Ormond Street Hospital, London, UK. [16]Department of Pediatrics, Aarhus University Hospital, Skejby, Aarhus, Denmark. [17]Institute of Pathology, Aalborg University Hospital, Aalborg, Denmark. [18]Department of Nephrology, Aalborg University Hospital, Aalborg, Denmark. [19]Department of Pediatrics and Adolescent Medicine, University of Freiburg Medical Center, Freiburg, Germany. [20]Department of Pediatric Nephrology, Hannover Medical School, Hannover, Germany. [21]Department of Pediatrics, Children's Hospital Lucerne, Lucerne, Switzerland. [22]Center of Pediatric Nephrology and Transplantation, Cairo University and Egyptian Group for Orphan Renal Diseases (EGORD), Cairo, Egypt. [23]Division of Nephrology and Hypertension, Mayo Clinic, Rochester, Minnesota, USA. [24]Center for Biological Signaling Studies (BIOSS), Freiburg, Germany. [25]Institute of Human Genetics, University Hospital of Cologne, Cologne, Germany. [26]Howard Hughes Medical Institute, Chevy Chase, Maryland, USA. [27]Center for Clinical Research, University of Freiburg, Freiburg, Germany. [28]These authors contributed equally to this work. Correspondence should be addressed to F.H. (friedhelm.hildebrandt@childrens.harvard.edu), C. Bergmann (carsten.bergmann@bioscientia.de) or S.S.L. (soeren.lienkamp@uniklinik-freiburg.de).

Received 11 February; accepted 3 June; published online 23 June 2013; doi:10.1038/ng.2681

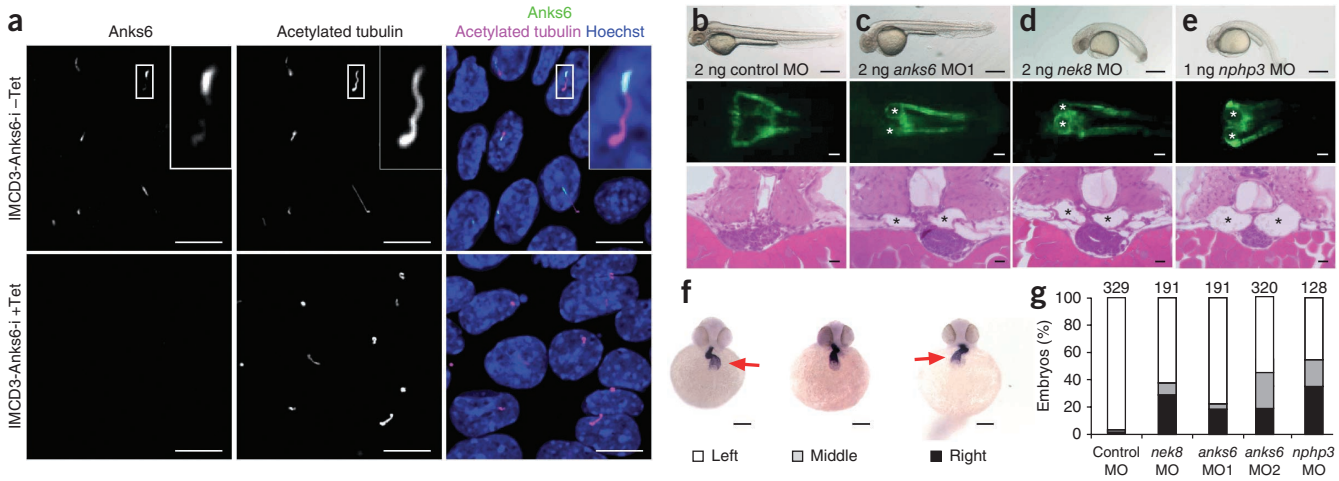

Figure 1 Anks6 localizes to the cilium, and knockdown results in pronephric cyst formation and laterality defects in zebrafish. (**a**) Confocal microscopy images of immunostaining for Anks6 in mouse IMCD3 cells showed localization to the proximal cilium. Tetracycline (Tet)-induced knockdown of *Anks6* confirmed the specificity of this signal. Cilia are stained with antibody to acetylated tubulin, and nuclei are stained with Hoechst. Insets each show one cilium (area enclosed by white boxes). Scale bars, 10 μm. (**b**–**e**) Zebrafish embryos injected with control morpholinos (MOs) (**a**) or with morpholinos targeting *nek8* (**b**), *anks6* (**c**) or *nphp3* (**d**) at 48 h post-fertilization (h.p.f.). Top, whereas the control embryos and *anks6* morphants did not show any malformation, *nek8* and *nphp3* morphants showed ventral body curvature. Scale bars, 100 μm. Middle, depletion of *anks6*, *nek8* or *nphp3* caused pronephric cyst formation (white asterisks). Scale bars, 50 μm. Bottom, histological sections were stained with hematoxylin and eosin; pronephric cysts are indicated by black asterisks. Scale bars, 10 μm. (**f**) Representative images of normal (left) and reversed (middle, right) heart looping in *anks6* morphants. *In situ* hybridization using the heart-specific probe *cmlc2* showed that heart laterality in zebrafish embryos deficient in *nek8* (2 ng of *nek8* MO), *anks6* (2 ng of *anks6* MO1, 3 ng of *anks6* MO2) or *nphp3* (1 ng of *nphp3* MO) was partially reversed (red arrows indicate atria). Scale bars, 100 μm. (**g**) Quantification of the percentage of embryos that showed laterality defects. The total number of each group of embryos analyzed is shown above the corresponding bar.

the NPHP2-NPHP3-NPHP9 module and the MKS module[5–7]. How specific complexes are assembled and how the composition of individual complexes is regulated are currently unknown.

NEK8, (*NPHP9*) encoding a NimA (never in mitosis A)-related serine-threonine kinase, is mutated in nephronophthisis. INVS recruits NEK8 and NPHP3 to the cilium and has only been shown to interact with NEK8 directly[7–9]. To obtain insight into the molecular function of NEK8 in nephronophthisis, we expressed NEK8 in human embryonic kidney (HEK 293T) cells and identified interacting proteins by mass spectrometry[10]. This approach identified ANKS6, a protein containing nine N-terminal ankyrin repeats and a C-terminal sterile α motif (SAM), as a potential binding partner (**Supplementary Table 1**); coimmunoprecipitation assays confirmed the interaction between NEK8 and ANKS6 (**Supplementary Fig. 1**). A missense mutation in *Anks6* (also known as *SamCystin* or *Pkdr1*) has recently been identified as the underlying cause of cystic kidney disease in the Han: SPRD cy/+ rat[11]. Anks6 was detected in the proximal segment of the cilium in mouse innermedullary collecting duct (IMCD3) cells

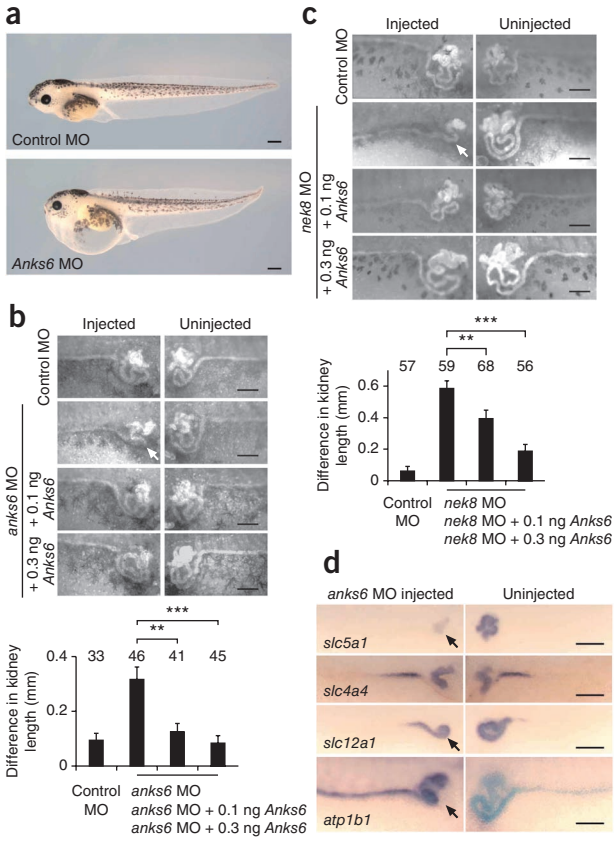

Figure 2 *Anks6* deficiency affects pronephros development in *Xenopus* embryos. (**a**) *Xenopus* embryos injected bilaterally with *anks6* morpholino developed edema in contrast to control embryos. Scale bars, 500 μm. (**b**) *Xenopus* morphants were stained with fluorescein-conjugated lectin to visualize pronephric epithelia after unilateral injection with *anks6* MO. Embryos injected with *anks6* morpholino showed strong simplification of proximal tubules (white arrow) in contrast to pronephros from uninjected embryos. The decrease in kidney length in the injected sides relative to the uninjected sides could be rescued by coinjection with rat *Anks6* mRNA. Scale bars, 200 μm. $^{**}P = 0.002$; $^{***}P \leq 0.001$, *t* test; error bars, s.e.m. (**c**) *nek8* deficiency (white arrow) phenocopies the pronephric phenotype of *anks6* deficiency and can be rescued by coexpression of rat *Anks6* mRNA. $^{**}P = 0.01$; $^{***}P \leq 0.001$, *t* test; error bars, s.e.m. (**d**) Whole-mount *in situ* hybridization for pronephric segment markers after unilateral injection with *anks6* morpholino. Expression of *slc5a1* (*SGLT-1K*), *slc12a1* (*NKCC2*) and *atp1b1* (*NA-K-ATPase*) was reduced on the side injected with *anks6* morpholino (black arrows). Scale bars, 200 μm. In **b**,**c**, the total number of each group of embryos analyzed is shown above the corresponding bar.

Table 1 Mutations of *ANKS6* in six families with PKD

Family: individual	Ancestry	Nucleotide alteration[a] (segregation)	Deduced protein change	Exon or intron (zygosity)	Continuous amino acid sequence conservation	Parental consanguinity	Renal phenotype	Extrarenal phenotype
A3121: 21	Egypt	c.934G>C (M: het, P: het)	p.Ala312Pro	Exon 4 (hom)	*Mus musculus*[c]	Yes	PKD, not enlarged Increased echogenicity (US) ESRD at 6 years	Heart, liver: not affected Other: died at 8 years Affected sibling: died *in utero*, presumed RF
B7397	Serbia	c.1322A>G (M: het, P: het)	p.Gln441Arg	Exon 6 (hom)	*Drosophila melanogaster*[d]	ND	PKD, not enlarged Increased echogenicity (US) CRF in early childhood	Heart, liver: not affected
A3114: 21	Iran	c.1973–3C>G (M: het, P: het)	3′ splice site (80% conserved)[b]	Intron 10 (hom)	No	Yes	PKD, not enlarged Increased echogenicity (US) ESRD at 2 years, RTX at 4 years	Heart: AS + PS Liver: periportal LF
B6794	Denmark	c.2054_2064del (M: het, P: het)	p.His685Profs*12	Exon 11 (hom)	No	ND	PKD, enlarged Increased echogenicity (US) ESRD at 1 year	Heart: AS Liver: periportal LF Other: delayed PMD
A649: 21	India	c.2370_2372delTCA (M: het, P: het)	p.Tyr790*	Exon 13 (hom)	No	No	PKD, enlarged Increased echogenicity (US) ESRD at birth	Heart: AS + HOCM, PDA Liver: cholestatic hepatopathy Other: SI, died at 4 months Affected sibling: died *in utero*, PKD, oligohydramnios
NPH316: 21, 22 and 23	Turkey	c.2512–2A>C (M: het, P: het)	3′ splice site	Intron 14 (hom)	No	Yes	21: PKD, enlarged ESRD at 25 years, RTX at 30 years 22: PKD, enlarged CRF at 16 years 23: PKD, enlarged CRF at 12 years	Heart: AS (23) Liver: not affected

AS, aortic stenosis; CRF, chronic renal failure; ESRD, end-stage renal disease; het, heterozygous; HOCM, hypertrophic obstructive cardiomyopathy; hom, homozygous; LF, liver fibrosis; ND, no data; M, maternal; P, paternal; PMD, psychomotor development; PS, pulmonary stenosis; PDA, patent ductus arteriosus; PKD, polycystic kidney disease; RTX, renal transplantation; RF, renal failure; SI, *situs inversus totalis*; US, ultrasound.
[a]cDNA mutations for *ANKS6* are numbered according to the human cDNA reference sequence NM_173551.3. Position 1 corresponds to the A of the ATG start translation codon. [b]G is not among the alternative nucleotides according to the consensus splice site (–3 acceptor splice site base: 80% C, 20% T). [c]Missense mutation predicted to be disease causing: PolyPhen-2 (score = 0.99). [d]Missense mutation predicted to be disease causing: MutationTaster ($P = 0.52$), PolyPhen-2 (score = 0.80); *Danio rerio*, Ala; *Ciona intestinalis*, Ser.

(**Fig. 1a** and **Supplementary Fig. 1**), similar to the localization of Invs, Nphp3 and Nek8 in this compartment[7,12]. To analyze the role of Anks6 during embryogenesis, we used morpholino (antisense oligonucleotide)-mediated depletion of *anks6* in zebrafish. Injection of two independent *anks6* morpholinos caused pronephric cyst formation (**Fig. 1b**,**c** and **Supplementary Fig. 2**). The cystic phenotype caused by *anks6* depletion in the pronephric tubule was identical to that seen in *nek8* and *nphp3* single morphants[13,14] (**Fig. 1d**,**e**), and pairwise combined knockdowns resulted in an additive effect on cyst formation (**Supplementary Fig. 2**). In addition, laterality defects, detected by *cmlc2* staining of early heart looping, were observed in *anks6*-depleted zebrafish and were comparable to those seen in embryos deficient in either *nphp3* or *nek8* (**Fig. 1f**,**g**).

Because unilateral injections allow tissue-restricted knockdown and analysis of organ-specific phenotypes, we used the *Xenopus* model to analyze the developmental events in renal formation in further detail. Both *nek8* and *anks6* are expressed during *Xenopus* development and are enriched within the proximal *Xenopus* pronephros at later developmental stages (**Supplementary Fig. 3**). Bilateral knockdown of *anks6* by morpholino (**Supplementary Fig. 4**) resulted in gross body edema that is typical of a renal excretory defect (**Fig. 2a**)[15,16], which was also observed with *nphp3* (**Supplementary Fig. 5**) and *invs* depletion[17]. Depletion of either *anks6* or *nek8* resulted in a notable simplification of the proximal pronephros convolute (**Fig. 2b**,**c**), a phenotype also previously reported with knockdown of *invs*[17]. Coexpression of morpholino-insensitive rat *Anks6* or *nek8* mRNA rescued the abnormalities, supporting the specificity of the observed phenotypes (**Fig. 2b** and **Supplementary Fig. 4**). The defects mediated by *nek8* morpholino were partially rescued by coexpression of *Anks6* mRNA (**Fig. 2c**). This finding suggests that the encoded proteins have common molecular effects, allowing Anks6 to partially substitute for Nek8. Early pronephric progenitor and later segmentation markers were not affected by *nek8* or *anks6* depletion (**Fig. 2d** and **Supplementary Fig. 5**). The reduced numbers of *slc5a1*- and *slc12a1*-positive pronephros segments indicated a shortening of the proximal and intermediate tubules (**Fig. 2d**). These data support the notion of overlapping roles for Nek8 and Anks6 during early tubular morphogenesis and are consistent with the phenotypic changes following *nphp3* (**Supplementary Fig. 5**) and *invs* depletion[17].

The above findings suggested that *ANKS6* might be involved in human cystic kidney disease presenting with a nephronophthisis-like clinical syndrome. Mutation analysis of our nephronophthisis cohorts identified eight individuals from six families with six different homozygous *ANKS6* mutations (**Table 1** and **Supplementary Figs. 6** and **7**), including two families with truncating mutations (c.2054_2064del, p.His685Profs*12 (B6794); c.2370_2372delTCA,

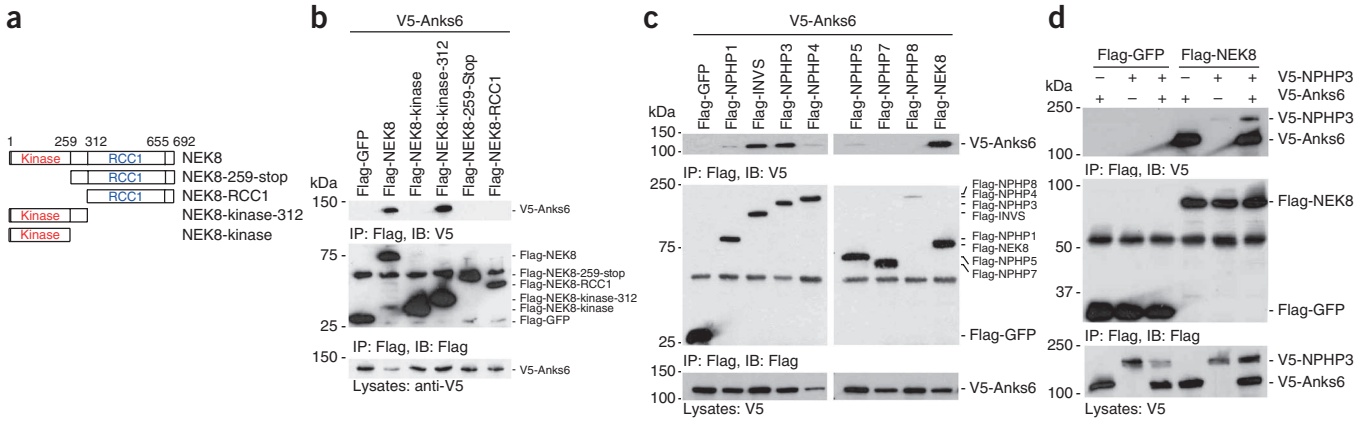

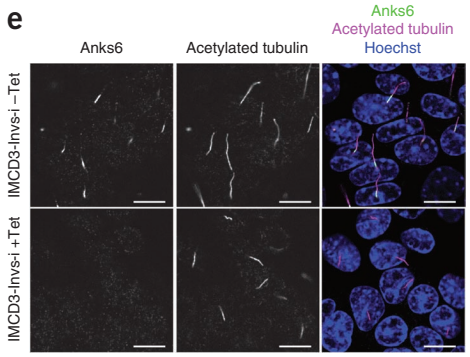

Figure 3 ANKS6 interacts with NEK8, INVS and NPHP3. (**a**) Schematic of NEK8 truncation mutants used for coimmunoprecipitation. NEK8 contains a kinase domain and a regulator of chromosome condensation (RCC1) domain. (**b**) Vector encoding V5-tagged full-length rat Anks6 was cotransfected into cells with vector encoding Flag-tagged full-length NEK8 or NEK8 truncation mutants. Anks6 precipitated with full-length NEK8 and the NEK8 truncation mutant containing the kinase domain up to amino acid 312 (kinase-312) in immunoprecipitation (IP) with an antibody to Flag. IB, immunoblot. (**c**) Anks6 precipitated with INVS, NPHP3 and NEK8 in immunoprecipitation with Flag-tagged NPHP proteins. (**d**) Flag-tagged NEK8 was coexpressed with V5-tagged NPHP3 and Anks6. NPHP3 was detected only in the precipitates from cells in which Anks6 was coexpressed. (**e**) Confocal microscopy images of mouse cells (IMCD3) with tetracycline-inducible knockdown of *Invs* stained for Anks6 and acetylated tubulin (to label cilia). Ciliary staining for Anks6 was lost in *Invs*-depleted cells. Hoechst stained nuclei. Scale bars, 10 µm.

p.Tyr790* (A649)), two families with splice-site mutations (c.1973–3C>G (A3114); c.2512–2A>C (NPH316)) and two families with non-synonymous missense mutations (c.934G>C, p.Ala312Pro (A3121); c.1322A>G, p.Gln441Arg (B7397)). All affected individuals had polycystic kidney disease (PKD) with early (infantile) onset, except for those in family NPH316 (juvenile onset). Whereas individuals with missense mutations showed non-enlarged cystic kidneys and no extrarenal manifestations, the splice-site and truncating mutations were associated not only with enlarged renal size but also with severe extrarenal defects such as hypertrophic obstructive cardiomyopathy, aortic stenosis, pulmonary stenosis, patent ductus arteriosus, *situs inversus* and periportal liver fibrosis (**Supplementary Fig. 6**). Only in family NPH316 (**Table 1** and **Supplementary Fig. 6**) did a splice-site mutation (c.2512–2A>C) not lead to early-onset end-stage renal disease (ESRD) and liver involvement, possibly owing to its location in intron 14, affecting splicing of only the last exon.

Structural heart defects are often associated with laterality defects and can result from defective cardiac looping during embryogenesis, which we observed in zebrafish embryos deficient for *Anks6*, *Nek8* and *Nphp3* (**Fig. 1f**,**g**). *INVS* and *NPHP3* mutations in humans cause ventricular and atrial septal defects, pulmonary and aortic stenosis and ventricular hypertrophy[18–20]. Four individuals with *ANKS6* mutations (A3114, B6794, A649 and NPH316) had aortic stenosis, causing obstructive cardiomyopathy in one case (A649); another (A3114) displayed additional pulmonary stenosis (**Table 1**), linking these three NPHP proteins by their clinical manifestations. The missense ANKS6 p.Gln441Arg alteration (B7397) did not alter the interaction of ANKS6 with other NPHP proteins or its ciliary localization (**Supplementary Fig. 7**), but the mutant protein did not rescue the renal phenotype in *Xenopus* knockdown embryos, confirming the clinical relevance of this mutation (**Supplementary Fig. 6**). These observations indicate that *ANKS6* encodes a new member of the NPHP family and is part of the phenotypically distinct NEK8-INVS-NPHP3 subgroup, which is characterized by structural heart defects in addition to infantile nephronophthisis and *situs inversus*.

To determine whether ANKS6 is part of a larger NPHP-associated protein network, we evaluated its interaction with other NPHP proteins. In NEK8, the kinase domain and the region between amino acids 259 and 312 was required for interaction with the ankyrin-repeat domain of rat Anks6 (**Fig. 3a**,**b** and **Supplementary Fig. 8**), which also recognized NPHP3 and INVS (**Fig. 3c**) but not the structurally related ankyrin-repeat protein Diversin (**Supplementary Fig. 8**). When NEK8 was precipitated from cells coexpressing INVS, the immobilization of INVS was strongly enhanced by the presence of Anks6 (**Supplementary Fig. 8**). Similarly, when NEK8 was coexpressed with NPHP3, Anks6 connected NEK8 with NPHP3 (**Fig. 3d**). Analysis of cilia in various tissues and model systems did not detect a role for ANKS6 in cilia formation or length control, but knockdown in *Xenopus* epidermal cells resulted in a mild defect in polarized orientation (**Supplementary Fig. 9**).

Juvenile cystic kidney (*jck*) mice carry a missense mutation in *Nek8*. Anks6 localization was identical in wild-type and *jck* mice, and the protein was even detectable in cyst lining cells (**Supplementary Fig. 9**). Consistent with a role for INVS in recruiting other NPHP proteins, endogenous Anks6 was lost from the proximal segment of cilia in *Invs*-depleted IMCD3 cells (**Fig. 3e**), with no effect on total Anks6 protein levels (**Supplementary Fig. 8**). Thus, ANKS6 not only acts as a central component of a distinct NPHP-associated module but seems to organize its assembly by linking INVS and NPHP3 to NEK8, and INVS is required to localize this complex to the proximal ciliary axoneme.

To further dissect the composition of the ANKS6-based module, we expanded our affinity proteomics screens using ANKS6 and different ANKS6 module partners as baits (**Supplementary Table 1**).

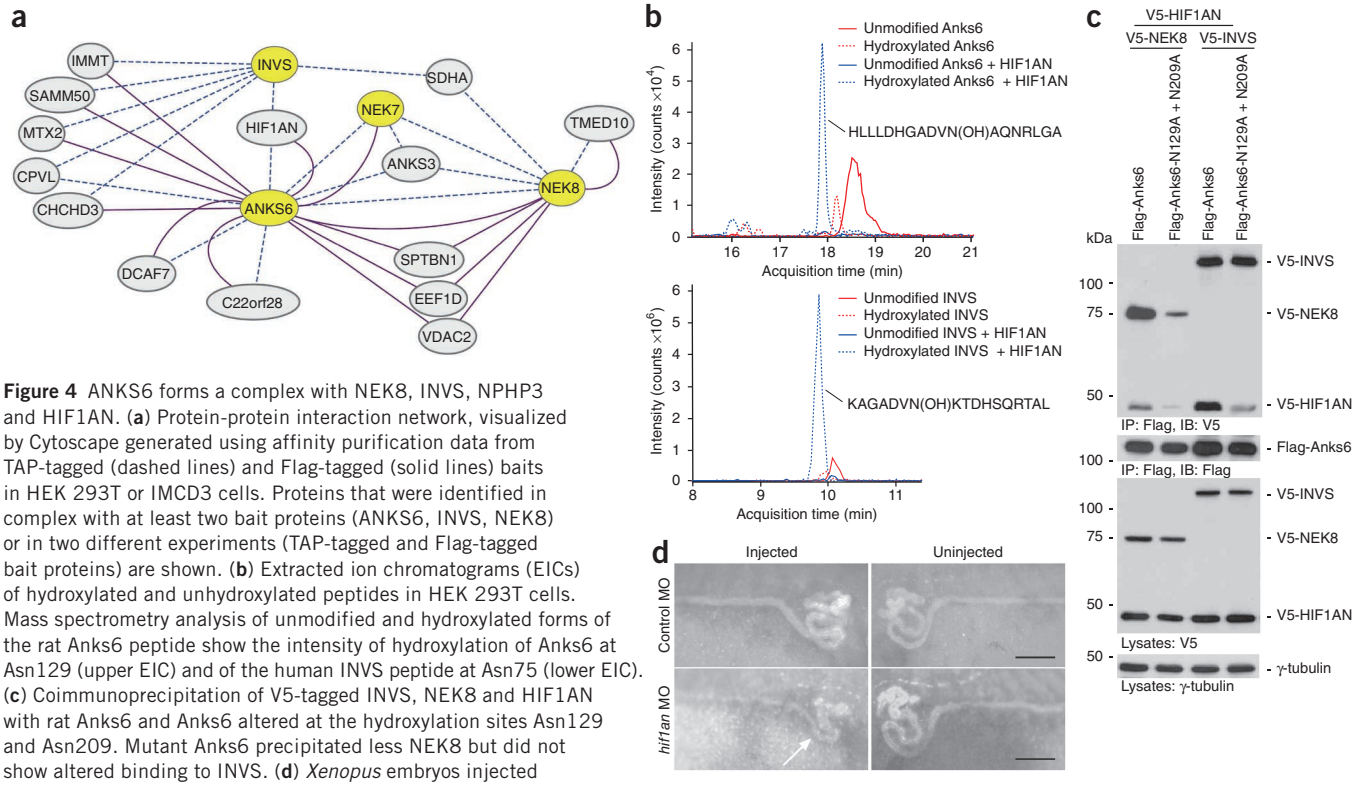

Figure 4 ANKS6 forms a complex with NEK8, INVS, NPHP3 and HIF1AN. (**a**) Protein-protein interaction network, visualized by Cytoscape generated using affinity purification data from TAP-tagged (dashed lines) and Flag-tagged (solid lines) baits in HEK 293T or IMCD3 cells. Proteins that were identified in complex with at least two bait proteins (ANKS6, INVS, NEK8) or in two different experiments (TAP-tagged and Flag-tagged bait proteins) are shown. (**b**) Extracted ion chromatograms (EICs) of hydroxylated and unhydroxylated peptides in HEK 293T cells. Mass spectrometry analysis of unmodified and hydroxylated forms of the rat Anks6 peptide show the intensity of hydroxylation of Anks6 at Asn129 (upper EIC) and of the human INVS peptide at Asn75 (lower EIC). (**c**) Coimmunoprecipitation of V5-tagged INVS, NEK8 and HIF1AN with rat Anks6 and Anks6 altered at the hydroxylation sites Asn129 and Asn209. Mutant Anks6 precipitated less NEK8 but did not show altered binding to INVS. (**d**) *Xenopus* embryos injected unilaterally with *hif1an* MO stained with fluorescein-conjugated lectin to visualize the pronephric tubules. Embryos injected with *hif1an* MO showed strong simplification of the pronephros on the injected side (arrow) in contrast to the uninjected side. Scale bars, 200 μm.

Integration of the ANKS6 screens with data from a proteomics screen of tandem affinity purification (TAP)-tagged NPHP-associated proteins (**Fig. 4a**) retrieved a subset of at least seven proteins with known mitochondrial localization and/or function and also identified the NEK family member NEK7 and the ankyrin-repeat protein ANKS3 as participants in this network. Because mutations of the mitochondrial X-prolyl aminopeptidase 3 gene (*XPNPEP3*) were recently found to cause a nephronophthisis-like syndrome[21], these proteins, including the mitochondrial components of the ANKS6 module, may represent additional candidates for nephronophthisis and related ciliopathies.

Mass spectrometry screens identified a consistent connection between ANKS6 and the asparaginyl hydroxylase HIF1AN (also known as FIH, factor inhibiting HIF), which was also identified after affinity purification of INVS (**Fig. 4a**). HIF1AN is an oxygen sensor that hydroxylates HIF-1α as well as other ankyrin-repeat proteins under normoxic conditions[22]. We confirmed the interaction of HIF1AN with INVS and ANKS6 but not with the ankyrin-repeat protein Diversin (**Supplementary Fig. 10**). Both INVS and ANKS6 contain well-defined and evolutionarily conserved hydroxylation recognition motifs (**Supplementary Fig. 10**); mass spectrometry detected peptides with hydroxylation at Asn75 of INVS and Asn129 of Anks6 (**Fig. 4b**). Coimmunoprecipitation experiments showed that HIF1AN facilitated formation of the ANKS6-INVS-NPHP3 module (**Supplementary Fig. 10**) and that alteration of the hydroxylation sites in ANKS6 resulted in decreased binding to NEK8 (**Fig. 4c**). These results suggest that hydroxylation of ANKS6 by HIF1AN influences complex formation by altering specific protein binding capacities. Hif1an is expressed in distal renal tubules[23], and knockdown of *hif1an* in *Xenopus* resulted in edema and tubular shortening (**Fig. 4d** and **Supplementary Fig. 10**), supporting a role for Hif1an in renal development. Hif-1α and its target genes are upregulated in cy/+ rat kidneys[24], and VEGF receptor inhibition results in cyst progression in these rats[25], suggesting that activation of the Hif-1α–dependent hypoxia pathway contributes to cyst progression in Anks6-deficient tubules. The ANKS6-INVS complex could compete with HIF-1α for hydroxylation by HIF1AN and induce a pseudohypoxic state when dysregulated. However, levels of HIF-1α were not affected by overexpression of Anks6 in renal epithelial cells (HEK 293T), excluding the possibility that expression levels of Anks6 alone affect hypoxia signaling (**Supplementary Fig. 10**). The response to chemically simulated hypoxia was also not affected under either condition (**Supplementary Fig. 10**).

Our study identifies ANKS6 as a new NPHP family member that assembles a distinct module of nephronophthisis-associated proteins, encompassing NEK8, INVS and NPHP3. The clinical findings as well as the *in vivo* data suggest that this network controls normal renal and cardiovascular development. HIF1AN connects the ANKS6 module to oxygen-dependent hydroxylation, which seems to alter the composition of the ANKS6-containing complex.

URLs. Cytoscape, http://www.cytoscape.org/; Renal Genes, http://www.renalgenes.org/.

METHODS

Methods and any associated references are available in the online version of the paper.

Note: Supplementary information is available in the online version of the paper.

ACKNOWLEDGMENTS

We are grateful to all patients and family members for their participation. We thank A. Sammarco, C. Engel, B. Müller, L. Schomas, S. Bräg and M. Klein for excellent technical assistance, the staff of the Life Imaging Center (LIC) in the Center for

Systems Biology, Albert-Ludwigs-University Freiburg for excellent confocal microscopy resources and the support in image recording and analysis, and U. Lanner and E. Haaf of the proteomics core facility. We thank N. Katsanis and J. Willer (Duke University) for providing us with expression constructs for NEK7 and INVS. We thank K. Coene for her help in generating affinity proteomics data for NEK8. We thank E. Jones for making the 3G8 and 4A6 antibodies available through the European *Xenopus* stock centre. V.F., T.E., H.J.B. and C. Bergmann are employees of Bioscientia, a member of Sonic Healthcare. D.B. is a Higher Education Funding Council for England (HEFCE) Clinical Reader and is supported by Kids Kidney Research. A.K.-Z., G.W., E.W.K., F.G., T.B.H. and S.S.L. are supported by the Deutsche Forschungsgemeinschaft (DFG; KFO 201). E.W.K. is supported by the DFG (KU 1504). C. Boehlke is supported by the Else-Kröner-Fresenius Stiftung. G.W. and T.B.H. are supported by the Excellence Initiative of the German Federal and State Governments (EXC 294-BIOSS). M.U., R.R. and G.W. are supported by the European Community's Seventh Framework Programme (grant agreement 241955, SYSCILIA). R.R. is supported by the Netherlands Organisation for Scientific Research (NWO Vidi-91786396 and Vici-016.130.664). K.B. and M.U. are supported by the European Community's Seventh Framework Programme under grant agreement 278568, PRIMES. This study was supported in part by the Excellence Initiative of the German Federal and State Governments (GSC-4, Spemann Graduate School) and by grants from the Agence Nationale de la Recherche to S.S. (R09087KS and RPV11012KK) and the Fondation pour la Recherche Médicale (DEQ20071210558). This research was supported by grants from the US National Institutes of Health to F.H. (DK068306 and DK090917). F.H. is an Investigator of the Howard Hughes Medical Institute, a Doris Duke Distinguished Clinical Scientist and a Frederick G.L. Huetwell Professor. C. Bergmann received support from the DFG (BE 3910/4-1, ZE 205/14-1 and SFB/TRR57), the Deutsche Nierenstiftung and the PKD Foundation.

AUTHOR CONTRIBUTIONS

S.H. performed *Xenopus* and biochemical experiments. D.E. performed zebrafish studies. C. Boehlke, C.S., T.Y., M.H. and M.M. analyzed cilia in various models. J.H., E.F., E.A.O., V.F., T.E., H.J.B., S.S., F.H. and C. Bergmann performed mutational analysis. J.v.R., T.-M.T.N., K.B., N.H., M.U. and R.R. performed affinity proteomic and network analyses. M.W.E., J.A.E.v.W., D.B., N.J.S., S.R., M.V., T.R., M.P., L.P., T.J.N., N.A.S.E., S.J.K. and P.C.H. recruited subjects and provided clinical information. S.H., D.E., T.Y., F.G., T.B.H., E.W.K., A.K.-Z., G.W. and S.S.L. designed experiments and analyzed data. S.H., J.H., R.R., S.S., C. Bergmann, F.H., G.W. and S.S.L. wrote the manuscript, with input from all authors.

COMPETING FINANCIAL INTERESTS

The authors declare no competing financial interests.

1. Hildebrandt, F. & Zhou, W. Nephronophthisis-associated ciliopathies. *J. Am. Soc. Nephrol.* **18**, 1855–1871 (2007).
2. Benzing, T. & Schermer, B. Clinical spectrum and pathogenesis of nephronophthisis. *Curr. Opin. Nephrol. Hypertens.* **21**, 272–278 (2012).
3. Hildebrandt, F., Benzing, T. & Katsanis, N. Ciliopathies. *N. Engl. J. Med.* **364**, 1533–1543 (2011).
4. Halbritter, J. *et al.* Identification of 99 novel mutations in a worldwide cohort of 1,056 patients with a nephronophthisis-related ciliopathy. *Hum. Genet.* published online; doi:10.1007/s00439-013-1297-0 (5 April 2013).
5. Sang, L. *et al.* Mapping the NPHP-JBTS-MKS protein network reveals ciliopathy disease genes and pathways. *Cell* **145**, 513–528 (2011).
6. Williams, C.L. *et al.* MKS and NPHP modules cooperate to establish basal body/transition zone membrane associations and ciliary gate function during ciliogenesis. *J. Cell Biol.* **192**, 1023–1041 (2011).
7. Shiba, D., Manning, D.K., Koga, H., Beier, D.R. & Yokoyama, T. Inv acts as a molecular anchor for Nphp3 and Nek8 in the proximal segment of primary cilia. *Cytoskeleton (Hoboken)* **67**, 112–119 (2010).
8. Fukui, H., Shiba, D., Asakawa, K., Kawakami, K. & Yokoyama, T. The ciliary protein Nek8/Nphp9 acts downstream of Inv/Nphp2 during pronephros morphogenesis and left-right establishment in zebrafish. *FEBS Lett.* **586**, 2273–2279 (2012).
9. Otto, E.A. *et al. NEK8* mutations affect ciliary and centrosomal localization and may cause nephronophthisis. *J. Am. Soc. Nephrol.* **19**, 587–592 (2008).
10. Gloeckner, C.J., Boldt, K., Schumacher, A., Roepman, R. & Ueffing, M. A novel tandem affinity purification strategy for the efficient isolation and characterisation of native protein complexes. *Proteomics* **7**, 4228–4234 (2007).
11. Brown, J.H. *et al.* Missense mutation in sterile α motif of novel protein SamCystin is associated with polycystic kidney disease in (*cy*/+) rat. *J. Am. Soc. Nephrol.* **16**, 3517–3526 (2005).
12. Shiba, D. *et al.* Localization of Inv in a distinctive intraciliary compartment requires the C-terminal ninein-homolog-containing region. *J. Cell Sci.* **122**, 44–54 (2009).
13. Liu, S. *et al.* A defect in a novel Nek-family kinase causes cystic kidney disease in the mouse and in zebrafish. *Development* **129**, 5839–5846 (2002).
14. Zhou, W., Dai, J., Attanasio, M. & Hildebrandt, F. Nephrocystin-3 is required for ciliary function in zebrafish embryos. *Am. J. Physiol. Renal Physiol.* **299**, F55–F62 (2010).
15. Tran, U., Pickney, L.M., Ozpolat, B.D. & Wessely, O. *Xenopus* Bicaudal-C is required for the differentiation of the amphibian pronephros. *Dev. Biol.* **307**, 152–164 (2007).
16. Satow, R., Chan, T.C. & Asashima, M. The role of *Xenopus* frizzled-8 in pronephric development. *Biochem. Biophys. Res. Commun.* **321**, 487–494 (2004).
17. Lienkamp, S. *et al.* Inversin relays Frizzled-8 signals to promote proximal pronephros development. *Proc. Natl. Acad. Sci. USA* **107**, 20388–20393 (2010).
18. Bergmann, C. *et al.* Loss of nephrocystin-3 function can cause embryonic lethality, Meckel-Gruber-like syndrome, situs inversus, and renal-hepatic-pancreatic dysplasia. *Am. J. Hum. Genet.* **82**, 959–970 (2008).
19. Tory, K. *et al.* Mutations of *NPHP2* and *NPHP3* in infantile nephronophthisis. *Kidney Int.* **75**, 839–847 (2009).
20. Chaki, M. *et al.* Genotype-phenotype correlation in 440 patients with NPHP-related ciliopathies. *Kidney Int.* **80**, 1239–1245 (2011).
21. O'Toole, J.F. *et al.* Individuals with mutations in *XPNPEP3*, which encodes a mitochondrial protein, develop a nephronophthisis-like nephropathy. *J. Clin. Invest.* **120**, 791–802 (2010).
22. Wilkins, S.E. *et al.* Factor inhibiting HIF (FIH) recognizes distinct molecular features within hypoxia-inducible factor-α (HIF-α) versus ankyrin repeat substrates. *J. Biol. Chem.* **287**, 8769–8781 (2012).
23. Schödel, J. *et al.* Factor inhibiting HIF limits the expression of hypoxia-inducible genes in podocytes and distal tubular cells. *Kidney Int.* **78**, 857–867 (2010).
24. Bernhardt, W.M. *et al.* Involvement of hypoxia-inducible transcription factors in polycystic kidney disease. *Am. J. Pathol.* **170**, 830–842 (2007).
25. Tao, Y. *et al.* VEGF receptor inhibition slows the progression of polycystic kidney disease. *Kidney Int.* **72**, 1358–1366 (2007).

ONLINE METHODS

High-throughput mutational analysis. Mutation analysis was performed by different approaches. First, we used PCR-based 48.48 Access Array microfluidic technology (Fluidigm) with subsequent next-generation sequencing. We applied a 14-fold primer multiplexing approach allowing PCR-based amplification of 672 amplicons (592 exons) for 48 DNA samples simultaneously in 13 known and 19 NPHP candidate genes, including *ANKS6*. We analyzed a total of 1,056 individuals with a nephronophthisis-related complex phenotype as described[4]. After 4 rounds of amplification and indexing of all 1,056 products derived from affected individuals with 384 different 10-bp barcodes in a subsequent PCR, we performed 2 × 150-bp bidirectional sequencing on 8 lanes of a Genome Analyzer IIx instrument (Illumina). Bioinformatic analysis was conducted using CLC-Genomics-Workbench software. Second, all exons and adjacent intronic boundaries of 129 genes (including *ANKS6*; 2,216 coding exons in total) known or hypothesized to cause ciliopathies were targeted by a custom SeqCap EZ choice sequence capture library (NimbleGen) and sequenced on a Roche454 GS FLX or an Illumina MiSeq platform (2 × 150-bp paired-end reads). We analyzed 268 individuals with a (poly)cystic kidney disease phenotype or a nephronophthisis-related complex ciliopathy with average coverage of 60-fold (GS FLX) or 120-fold (MiSeq). Bioinformatics analysis was performed using Roche GS Reference Mapper software (v2.6), SeqPilot SeqNext module (v3.5.2, JSI medical systems) and an in-house bioinformatics pipeline. For both approaches, potential mutations were confirmed by Sanger sequencing and shown to segregate. Linkage analysis using Affymetrix 250k SNP arrays was performed on a consanguineous family with nephronophthisis (family NPH316). Four unaffected and two affected children are the offspring of a first-cousin marriage, and one unaffected and two affected children are the offspring of a third-cousin marriage. DNA samples from the third-cousin parents and their two affected children and a sample from their affected cousin were available for the study. Haplotype analysis was performed with MERLIN software. Mutation analysis of *ANKS6* was performed by Sanger sequencing. We obtained blood samples, pedigrees and clinical information after receiving informed consent (http://www.renalgenes.org/). Approval for experiments on humans was obtained from the University of Michigan Institutional Review Board and the other institutions involved. Diagnosis with nephronophthisis-related ciliopathies was based on published clinical criteria[20].

Animals and maintenance. *Xenopus* embryos were cultured, manipulated and staged as described[17]. Zebrafish (strain *Tg*(*wt1b*:*GFP*))[26] were bred and maintained under standard conditions at 28.5 °C. C57BL/6J-Nek8jck/J mice were purchased from The Jackson Laboratory, and homozygous and wild-type mice were derived from matings of heterozygous animals. All experiments were approved by the institutional animal committee (Regierungspräsidium Baden-Württemberg).

RNA extraction and RT-PCR. RNA was isolated from *Xenopus* and zebrafish embryos following the RNeasy manual (Qiagen), and cDNA synthesis was performed using the RevertAid H Minus kit (Fermentas) and the First-Strand cDNA Synthesis kit (Invitrogen). Primer sequences are given in **Supplementary Table 2**.

Embryo microinjection manipulations. We performed 10-nl microinjection in *Xenopus* ventrolateral vegetal blastomeres to target the pronephros anlagen at the four- to eight-cell stage. *GFP* or *RFP* mRNA was coinjected as an injection control, and only fluorescent embryos were used for further analysis. For zebrafish knockdown experiments, morpholinos and sense RNA were diluted in 0.1 M KCl to concentrations of 1–4 μg/μl and 0.1 μg/μl, respectively. We injected 1 nl of the dilution through the chorion of embryos at the one- or two-cell stage[27]. The sequences of antisense oligonucleotide morpholinos (GeneTools) are provided in **Supplementary Table 3**. The TNT Quick Coupled Transcription/Translation System (Promega) was used to confirm morpholino efficiency. *In vitro* synthesis of mRNA was performed using the mMessage mMachine kit (Ambion) as follows: xNek8_VF10: PstI, T7; rat Anks6_VF10: SalI, T7; hNPHP3_VF10: SalI, T7; and hHIF1AN_VF10: SalI, T7.

Whole-mount *in situ* hybridization. Whole-mount *in situ* hybridization was performed with digoxigenin-labeled antisense probes as described[17,27]. For *in situ* probes, the plasmids were linearized and transcribed with SP6 or T7 (Roche). Antibody to digoxigenin conjugated to alkaline phosphatase was used to detect bound probes (Roche, 11093274910). Whole-mount *in situ* hybridization for *cmlc2* was performed in zebrafish embryos 48 h.p.f.

Histology. Zebrafish embryos were embedded in Technovit 7100 (Heraeus), stained with hematoxylin and eosin and imaged with an Axioplan2 microscope and AxioVision software (Zeiss). Wild-type and Nek8/jck mice were sacrificed at the indicated time points, and kidneys were collected after perfusion with 4% paraformaldehyde (PFA) via the renal artery and subsequently immersion fixated at 4 °C overnight. Paraffin sectioning was performed using standard techniques.

Immunofluorescence staining and microscopy. Zebrafish embryos were fixed in 4% PFA and 1% DMSO overnight at 4 °C, equilibrated in 100% methanol at −20 °C for 1 h, digested with proteinase K (10 μg/ml) for 20 min, treated with ice-cold acetone for 5 min at −20 °C and incubated in blocking solution (1% PBSTT, 1% DMSO, 2% sheep serum and 1% BSA). Embryos were then incubated with antibody to acetylated tubulin (Sigma-Aldrich, T6793; 1:3,000 dilution).

For fluorescent staining of whole *Xenopus* embryos, we used 3G8 and 4A6 antibodies (European *Xenopus* stock center; 1:2 dilutions). For *Xenopus* rescue experiments, whole embryos were stained with fluorescein-conjugated *Lycopersicon esculentum* lectin (LEL) (Vector Laboratories; 1:1,000 dilution). Kidney length was measured using ImageJ. The difference in kidney length in the uninjected and morpholino-injected sides was calculated. Analysis of basal body polarization in *Xenopus* epidermal cells was performed as described[28].

Immunofluorescence staining of IMCD3 cells was carried out after cells were fixed using 4% PFA or methanol-acetone (1:1). Cells were permeabilized with 0.1% Triton X-100 in PBS and incubated in blocking solution (5% horse serum or 0.2% goldfish gelatine). Primary antibodies included rabbit antibody to ANKS6 (Sigma-Aldrich/Prestige Antibodies, polyclonal antibody, HPA008355), mouse antibody to acetylated tubulin (Sigma-Aldrich, T6793; 1:3,000 dilution), mouse antibody to γ-tubulin (Sigma-Aldrich, T6557) and Hoechst 33342. Antibodies were visualized using Cy5-, Cy3- or Alexa488–labeled secondary antibodies at a dilution of 1:1,000 (Jackson ImmunoResearch).

For the ciliogenesis assay, IMCD3 cells were grown on glass for 6 d, stained for acetylated tubulin and Hoechst, and imaged with a confocal microscope. *z* stacks were generated to include all cilia in different *z* positions and were then projected to one plane (maximum intensity projection). Experiments were conducted three independent times (with five fields of view per *N*).

Confocal imaging was performed with an LSM 510 Duo-Live microscope equipped with a 100×/1.45 NA Plan-Apochromate objective (both from Carl Zeiss). Excitation of the fluorophores (Hoechst 33342, Alexa488, Cy3 and Cy5) was performed at 405, 488, 561 and 633 nm, respectively. For detection of the emission signal at specified ranges, the photomultiplier channels were used with BP filter 420–480, BP filter 505–530, BP filter 575–615 and LP filter 650 nm. Confocal pinhole diameters were adjusted to 1-μm sections. In each cell, the cilia and nucleus were projected onto one plane.

Antigen retrieval on paraffin-embedded slides of mouse kidneys was performed using citrate buffer (10 mM trisodium citrate dihydrate, pH 6.0) in a steamer for 30 min. The following primary antibodies were applied: antibody to Anks6 (Sigma-Aldrich; 1:100 dilution) and antibody to acetylated tubulin (Sigma-Aldrich, monoclonal antibody, clone 6-11B-1; 1:400 dilution). Primary antibodies were used in a consecutive staining procedure to avoid cross-reactions. Secondary antibodies included Alexa488 and Alexa555 (diluted 1:500) and Hoechst 33342 (diluted 1:1,000) (Jackson ImmunoResearch). Slides were mounted with ProLong Gold Antifade (Invitrogen). Images were acquired on a confocal Zeiss LSM 510 upright microscope equipped with a Plan-Apochromat 63×/1.4 NA oil M27 objective. All confocal image recording was performed with Zen black Software (Zeiss).

Plasmids, reagents and expression clones. The Rapid Amplification of cDNA Ends kit (Invitrogen) was used to synthesize the 5′ end of *Xenopus Nek8*. Full-length *NEK8* (NM_178170.2) and several truncated versions of *NEK8* created by PCR and standard cloning techniques were fused to a pcDNA6

vector encoding a V5 or Flag tag (Invitrogen). Full-length *Anks6* cDNA clones (NM_ 001015028 and NM_173551.3) were synthesized by OriGene and fused to a pcDNA6 vector encoding a V5 or Flag tag. When using the RTS 100 Wheat Germ Continuous Cell-Free System (5Prime), we cloned the DNA of interest into the pIVEX1.4 WG vector. An entry clone for *NEK8* was created by PCR using a *NEK8* cDNA IMAGE clone corresponding to NCBI RefSeq accession NM_178170.2. A *NEK8* expression construct was created using Gateway technology (Invitrogen). *NEK7* (matching NCBI RefSeq accession NM_133494.2) and *INVS* (matching Ensembl accession ENST00000374921) expression constructs for affinity proteomics were kindly provided by N. Katsanis and J. Willer.

Cell culture, coimmunoprecipitation, protein blotting and antibodies. Human embryonic kidney (HEK 293T) cells (purchased from the American Type Culture Collection (ATCC)) were transiently transfected, and coimmunoprecipitation was carried out as described[28]. Briefly, cells were washed with PBS, lysed with lysis buffer (1% Triton X-100, 20 mM Tris, pH 7.5, 50 mM NaCl, 50 mM NaF, 15 mM $Na_4P_2O_7$ and 0.1 mM EDTA) supplemented with 2 mM Na_3VO_4 and protease inhibitor mix (Roche). Lysates were incubated with anti-Flag M2 agarose Affinity M2 beads for 2 h and washed with lysis buffer.

For tetracycline-inducible (1 μg/ml) *Anks6* knockdown (Anks6-i), inner medullary collecting duct (IMCD3) cells were lentivirally transduced with a short hairpin RNA (shRNA) targeting base pairs 2304–2324 of the coding sequence of mouse *Anks6* (NM_001024136), which was cloned into pLVTH. The efficiency of the knockdown was verified by quantitative RT-PCR (qPCR) with MesaFast qPCR Master Mix Plus for SYBR Assay (Eurogentec). The *Invs* IMCD3 knockdown cell line (Invs-i) was lentivirally transduced with a tetracycline-inducible shRNA targeting base pairs 945–965 of the coding sequence of mouse *Invs* (NM_010569), and efficiency was verified by qPCR. For overexpression, rat *Anks6* (and sequence encoding rat Anks6 Gln433Arg) was cloned into pLXSN in an orientation to allow translation in frame with C-terminal Venus, and the construct was transduced into IMCD3 cells. Hypoxic conditions were mimicked using $CoCl_2$ (Sigma-Aldrich) with a final concentration of 125 μM for 8 h. Protein blots were analyzed with antibodies to HIF-1α (BD Biosciences), clone 54/HIF-1α 1:1,000 dilution), ANKS6 (Sigma-Aldrich/Prestige Antibodies, polyclonal antibody, HPA008355; 1:1,000 dilution) and γ-tubulin (Sigma-Aldrich, T6557; 1:3,000 dilution).

Scanning electron microscopy. For scanning electron microscopy, samples were fixed with 4% glutaraldehyde (Sigma-Aldrich, EM quality grade) for 4 d at 4 °C and were subsequently dehydrated (in 50%, 70%, 80%, 90% and 100% ethanol; 1:1 ethanol and HMDS for 1 h; and 100% HMDS for 30 min; afterwards, solvent was allowed to evaporate). After dehydration, standard coating was performed with gold (Zeiss Semco Nanolab7, Polaron Cool Sputter Coater E 5100, Balzer Cpd 020). Image acquisition of respective *Xenopus* embryos was performed using a Leo 1450 VP scanning electron microscope.

Affinity proteomics. Strep-Flag tandem affinity purification (SF-TAP) was performed as described[29]. Before liquid chromatography tandem mass spectrometry analysis, protein precipitates were subjected to tryptic proteolysis. Mass spectrometry analysis of SF-TAP–purified samples was performed as described. Digested samples were separated on an UltiMate 3000 RSLCnano system, on-line coupled to an LTQ Orbitrap Velos (Thermo Fisher Scientific). All samples for tandem mass spectrometry were analyzed using Mascot (version 2.4, Matrix Science). Mascot was set up to search the human subset of the SwissProt database (Release 2012_05; 20,245 entries), assuming trypsin as the digestion enzyme. Mascot was searched with a fragment ion mass tolerance of 1.00 Da and a parent ion tolerance of 10.0 PPM. Oxidation of methionine was specified as variable modification, iodoacetamide derivative of cysteine as fixed. Mascot results were loaded in Scaffold (version Scaffold_3.5, Proteome Software) to validate tandem mass spectrometry–based peptide and protein identifications. Peptide identifications were accepted if they could be established at greater than 80.0% probability, as specified by the Peptide Prophet algorithm[30]. Protein identifications were accepted if they could be established at greater than 95.0% probability and contained at least two identified peptides. Protein probabilities were assigned by the Protein Prophet algorithm[31]. Proteins that contained similar peptides and could not be differentiated on the basis of tandem mass spectrometry analysis alone were grouped to satisfy the principles of parsimony.

For immunoprecipitation of Flag, washed immunoprecipitates were incubated with Flag peptide (Sigma) to elute the precipitated protein from the beads coated with antibody to Flag. Samples were separated by SDS gel and stained, and in-gel digests were performed as described in standard protocols. Digests with different proteases (trypsin, elastase and thermolysin) were performed in 0.1 M NH_4HCO_3 (pH 8) overnight at 37 °C. For each gel band, about 0.1 μg of protease was used. Peptides were extracted from the gel slices using 5% formic acid. All liquid chromatography tandem mass spectrometry analyses were performed on an ion-trap mass spectrometer (Agilent 6340, Agilent Technologies) coupled to a 1200 Agilent nanoflow system via an HPLC-Chip cube ESI interface. Alternatively, liquid chromatography tandem mass spectrometry analyses were performed on a Q-TOF mass spectrometer (Agilent 6520, Agilent Technologies) coupled to a 1200 Agilent nanoflow system via an HPLC-Chip cube ESI interface. Peptides were eluted with a linear acetonitrile gradient with 1% of acetonitrile added per minute at a flow rate of 300 nl/min (starting with 3% acetonitrile). For raw data processing, Mascot Distiller 2.4.2 (Matrix Science) was used. Data from the Mascot searches were further condensed for the samples (experimental and control) in Scaffold 3.4.9 (Proteome Software).

Statistical analyses. SigmaStat software was used to analyze statistical significance. All experiments were performed three times, and plots show mean ± s.e.m. The tests used to calculate the significance are indicated in the corresponding figure legends for the individual experiments. Standard numbers of embryos (20 to 30 for *Xenopus*, 100 for zebrafish) were injected per experiment, and non-viable embryos were excluded before gastrulation. The number of analyzed embryos is given above each bar.

26. Perner, B., Englert, C. & Bollig, F. The Wilms tumor genes *wt1a* and *wt1b* control different steps during formation of the zebrafish pronephros. *Dev. Biol.* **309**, 87–96 (2007).
27. Epting, D. *et al.* The Rac1 regulator ELMO1 controls vascular morphogenesis in zebrafish. *Circ. Res.* **107**, 45–55 (2010).
28. Ganner, A. *et al.* Regulation of ciliary polarity by the APC/C. *Proc. Natl. Acad. Sci. USA* **106**, 17799–17804 (2009).
29. Boldt, K., van Reeuwijk, J., Gloeckner, C.J., Ueffing, M. & Roepman, R. Tandem affinity purification of ciliopathy-associated protein complexes. *Methods Cell Biol.* **91**, 143–160 (2009).
30. Keller, A. *et al.* Experimental protein mixture for validating tandem mass spectral analysis. *OMICS* **6**, 207–212 (2002).
31. Nesvizhskii, A.I., Keller, A., Kolker, E. & Aebersold, R. A statistical model for identifying proteins by tandem mass spectrometry. *Anal. Chem.* **75**, 4646–4658 (2003).

doi:10.1038/ng.2681